forests

MDPI

Article

Predictive Models for Elastic Bending Behavior of a Wood Composite Sandwich Panel

Mostafa Mohammadabadi [1], James Jarvis [2], Vikram Yadama [3,*] and William Cofer [3]

[1] Material Science and Engineering Program and Composite Materials and Engineering Center, Washington State University, Pullman, WA 99164, USA; m.mohammadabadi@wsu.edu
[2] DCI Engineers, San Francisco, CA 94105, USA; jjarvis@dci-engineers.com
[3] Department of Civil and Environmental Engineering and Composite Materials and Engineering Center, Washington State University, Pullman, WA 99164, USA; wcofer@wsu.edu
* Correspondence: vyadama@wsu.edu; Tel.: +1-509-335-6261

Received: 24 April 2020; Accepted: 22 May 2020; Published: 1 June 2020

Abstract: Strands produced from small-diameter timbers of lodgepole and ponderosa pine were used to fabricate a composite sandwich structure as a replacement for traditional building envelope materials, such as roofing. It is beneficial to develop models that are verified to predict the behavior of these sandwich structures under typical service loads. When used for building envelopes, these structural panels are subjected to bending due to wind, snow, live, and dead loads during their service life. The objective of this study was to develop a theoretical and a finite element (FE) model to evaluate the elastic bending behavior of the wood-strand composite sandwich panel with a biaxial corrugated core. The effect of shear deformation was shown to be negligible by applying two theoretical models, the Euler–Bernoulli and Timoshenko beam theories. Tensile tests were conducted to obtain the material properties as inputs into the models. Predicted bending stiffness of the sandwich panels using Euler-Bernoulli, Timoshenko, and FE models differed from the experimental results by 3.6%, 5.2%, and 6.5%, respectively. Using FE and theoretical models, a sensitivity analysis was conducted to explore the effect of change in bending stiffness due to intrinsic variation in material properties of the wood composite material.

Keywords: small-diameter timber; wood-strand composite; sandwich panel; bending stiffness; finite element model; theoretical model; building envelope

1. Introduction

Increasing world population and limited natural resources require us to rethink how we utilize our forests more productively to construct effective building products for houses. Forests play a critical role in sequestering carbon and building products and can further this cause by continuing to store the carbon for a prolonged period. As an order of magnitude, a tree on an average absorbs one ton of CO2 and produces 0.7 tons of O2 for every cubic meter of growth [1], and every cubic meter of wood as a building material can reduce CO2 emissions by an average of 2 tons compared to other building materials such steel and concrete [2]. A sustainable forest management plan to protect forests against fire, insects, and disease should consider thinning operations that result in improving forest health. Often, this requires the removal of small-diameter timber (SDT) at a cost and requires high-value markets or high-volume usage of these low-quality logs to recover the forest treatment costs. For example, the average cost for a forest service thinning (approximately $70/dry ton) is usually more than the market value of the SDT removed (energy and chip markets pay approximately $25 to $35/dry ton) [3]. Besides existing products such as medium-density fiberboard (MDF) and oriented strand board (OSB) produced from SDT, it is worth developing new products by converting

these low-quality SDTs into more robust and versatile building products that would meet the structural performance as well as energy requirements.

Sandwich structures are widely used in many areas like aerospace, automotive, civil, building construction, and marine industries because their clever construction reduces their weight while increasing their mechanical performance [4]. However, those with hollow cores have attracted interest from researchers because the hollow geometry of the core can be used to improve the thermal performance when they are filled with appropriate materials, such as closed-cell foam. This idea has also been used to develop wood-based sandwich panels with different 3D core geometries [5–10]. Some of the disadvantages of these panels is that they use a wet forming process for panel manufacturing, have a relatively low structural capacity, and have poor interfacial shear strength at the intersection between the core and face plies resulting in poor structural performance. Voth et al. [11] designed a 3D core with biaxial corrugated geometry and used wood strands produced from SDT to fabricate the panel shown in Figure 1. The bending behavior of wood-strand-based sandwich panels with biaxial corrugated core geometry was investigated experimentally, and the results showed the stiffness in both directions along the length and width is higher than that of oriented strand board (OSB) and 5-ply plywood. Additionally, sandwich panels with cavities filled with insulation foam decreased the thermal conductivity of the panels by over 17% while improving the panel strength and stiffness by 34 and 16 percent [12]. Creep [13] and impact [14] performances of the biaxial corrugated core sandwich panel were also investigated experimentally.

For application of these sandwich panels as a structural component in building envelopes (roofs, floors, and walls) with longer spans, the bending stiffness and the bond area between the core and the faces need to be increased as they typically limit the load-carrying capacity. Models to predict their behavior are useful tools to design and engineer the geometry of cores and sandwich panels as long as they are verified and validated. Additionally, it is critical to accurately determine the material properties that serve as inputs to these models. The finite element method is an effective way to simulate complicated geometries under different loading and boundary conditions to predict the behavior and explore distribution of stress and strain in the structures. It is also useful to develop theoretical models to derive closed-form solutions to understand the influence of material properties and geometrical features on the behavior of the structures. These models can then be used to analyze the behavior of structural components subjected to service loads. In this study, a finite element model and a theoretical model were developed to evaluate the bending behavior of a wood-strand composite sandwich panel with a biaxial corrugated core geometry designed by Voth [11]. Elastic constants of the wood-strand composite material required to develop both the finite element (FE) and the theoretical models were evaluated, and the models were verified against the experimental results. Considering the intrinsic nature of wood, the models were further applied in a sensitivity analysis to understand the influence of variation in elastic constants on the bending stiffness of the sandwich panel.

2. Materials

Using a disc-strander (manufactured by CAE) operating at a rotational speed of 500 rpm (shown in Figure 1a), thin wood strands with an average thickness of 0.36 mm were produced from ponderosa pine (pp) logs ranging in diameter from 191 to 311 mm. Wood strands were then dried to a target moisture content of 3%–5% and sprayed with an aerosolized liquid phenol formaldehyde (PF) resin in a drum blender (shown in Figure 1b) to a target resin content of 8% of the oven-dry weight of the wood strands. Subsequently, wood strands sprayed with resin were oriented and hand-formed unidirectionally using a forming box (shown in Figure 1c) to fabricate a wood strand mat, or preform, as shown in Figure 1d. Unidirectional mats were consolidated to a thickness of 6.35 mm into flat panels for the outer plies or corrugated core panels (shown in Figure 1f) with a matched-die mold (shown in Figure 1e) in a hot press. For both flat and corrugated panels, the preform was hot-pressed for 6 minutes at an operating temperature of 160 °C to reach a target thickness of 6.35 mm. Applied pressure by the press was an uncontrolled variable and was dependent on the density and the target thickness of the panel. To fabricate the sandwich panels as shown in Figure 1f–h, flat panels were

then bonded with a two-part epoxy resin (Loctite Epoxy by Henkel) to the biaxial corrugated cores. A 400-grit sandpaper was used for a light sanding of the bonding area of both the flat and corrugated panels. A thin layer of resin was only applied to both sides of the corrugated core. Flat panels were placed on both sides of the corrugated core to form a sandwich panel as shown in Figure 1g, and the panels were clamped for 24 hours before cutting and trimming.

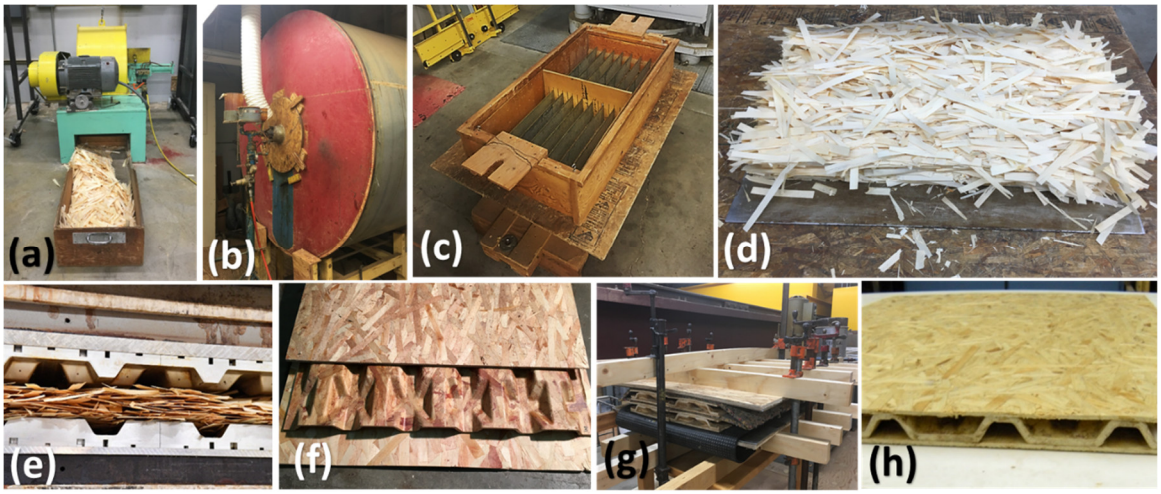

Figure 1. Fabrication process: (**a**) disc-strander, (**b**) blender, (**c**) orientor, (**d**) preform, (**e**) hot-pressing using mold, (**f**) components of sandwich panel, (**g**) clamped panels, and (**h**) sandwich panel.

A unit cell (UC), the simplest repeating element of the biaxial corrugated core geometry, along with its dimensions, is given in Figure 2a. Directions along the length and width of the panel are defined as longitudinal and transverse directions. Wood strands were oriented along the longitudinal direction to make the preform for both the corrugated core and the flat panels.

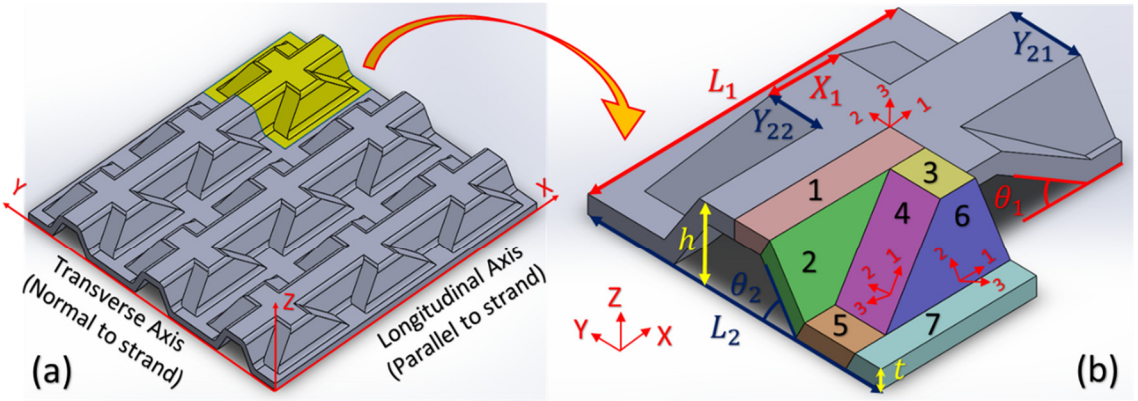

h	t	L_1	L_2	θ_1	θ_2	X_1	Y_{21}	Y_{22}
25	6.4	114	108	30	56	23	19	19

Figure 2. Biaxial corrugated core (**a**) highlighted unit cell (**b**) geometric parameters and their values in mm.

L_1, L_2, and h are the length, width and height of the UC. Core wall thickness was defined as t. Y_{21}, Y_{22}, and X_1 are associated with the dimensions of the bonding area between the flat panels and the core to fabricate a sandwich panel. The angle of slanted areas is represented by θ_1 and θ_2 as shown in Figure 2b.

3. Experiments

This section is divided into two subsections. The first introduces the experiments conducted to establish material properties employed in the FE and theoretical models. The second part describes

the experimental bending tests performed to verify the sandwich panel bending stiffness predictions of the FE and theoretical models.

3.1. Tensile Test

Wood is an orthotropic material and requires nine elastic constants to be fully defined [15]. However, because the fiber orientation in individual strands varies in the width direction with respect to an idealized orthotropic material axes and the preform is a conglomeration of wood strands oriented uniaxially, transverse isotropy was assumed to define the material properties of both flat plies and the core [16]. Therefore, five elastic constants, including E_1, $E_2 = E_3$, $G_{12} = G_{23}$, $\nu_{12} = \nu_{13}$, and ν_{23}, were required to fully define the sandwich panel. Subscripts 1, 2, and 3 refer to the material axes (local coordinate system) of the composite material (Figure 2b). The 2–3 plane is the plane of isotropy for this transversely isotropic material. To determine these representative material properties, tension specimens shown in Figure 3a were cut from flat panels at different angles (0°, 15°, and 90°) with respect to the longitudinal axis (x axis in Figure 2) and tested (Figure 3b) as per the standard testing guidelines in ASTM D1037 [17]. Testing was performed using an 8.8-kN Instron test frame Model 4466, change in gauge length (elongation) was recorded using a 25-mm Epsilon extensometer, and then strain measurements were obtained by dividing the elongation by the initial gauge length (25 mm).

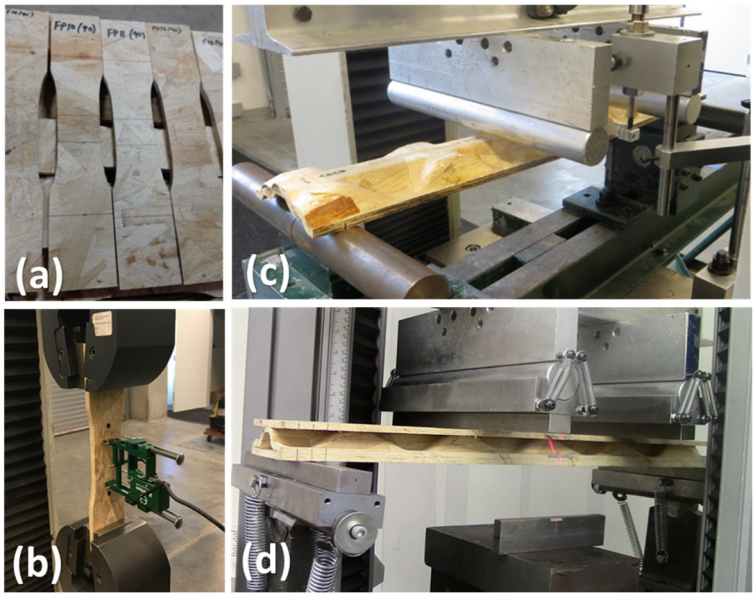

Figure 3. Mechanical testing: (**a**) tension specimens, (**b**) tensile testing, (**c**) bending of corrugated core, and (**d**) bending of sandwich beam.

Longitudinal and transverse Young modulus (E_1 and E_2) were obtained from test results of 0° and 90° specimens, respectively. These material properties, along with the test results of coupons prepared at 15° angles, were used to determine the shear modulus, G_{12}, using the transformation equation [15].

$$G_{12} = \left[\frac{2\upsilon_{12}}{E_1} + \frac{\frac{1}{E_\theta} - \frac{cos^4\theta}{E_1} - \frac{sin^4\theta}{E_2}}{(sin^2\theta)(cos^2\theta)} \right]^{-1} \quad (1)$$

where E_1, E_2, E_θ, υ_{12}, and θ are modulus of elasticity in the longitudinal, transverse, and θ-directions, Poisson's ratio, and assumed angle in this study (15°), respectively. The value for Poisson's ratio, υ_{12}, was assumed to be 0.358, based on a previous study [18] which evaluated the mechanical properties of a wood strand composite material with similar structure and manufacturing process to the composite material used in this study. Among commercially produced wood-strand-based materials,

structural composite lumber (SCL) [e.g., parallel strand lumber (PSL), oriented strand lumber (OSL), and laminated strand lumber (LSL)] are similar to the material in this study. They are manufactured using long veneer strips or wood strands that are also aligned in a longitudinal direction. Therefore, Poisson's ratio, υ_{23}, of PSL as determined by Clouston [19] was assumed for the material of interest in this study. Considering the transverse isotropy assumption resulting in material isotropy in plane 2–3, G_{23} was calculated as:

$$G_{23} = \frac{E_2}{2(1+\upsilon_{23})} \quad (2)$$

Since wood is a natural material influenced by variations in growing conditions, its properties are influenced by naturally occurring growth characteristics, such as knots, variation in cell wall thickness between the annual rings, and grain deviations [20]. This inherent variability can significantly influence the properties of wood strands produced from logs or lumber, and this variation in turn can affect the properties of the composite material produced using these strands. Furthermore, variations in the mat architecture can also be expected due to variation in the orientation of the wood strands with respect to the longitudinal axis as the mat is formed. In addition, mat architecture would also influence the heat and mass transfer during the hot-pressing process due to variations in moisture and heat distribution within a mat [21]. Effort was made to reduce these variations by tightly controlling the processing variables and the press schedule during the production process. Yet, variation in density within a panel and between the panels after consolidation is inevitable and should be expected. As mentioned, this variation in density can affect the material properties obtained from tensile test. To explore the influence of density on the longitudinal modulus, panels with density varying between 600 and 950 kg/m^3 were fabricated and submitted to tensile test.

3.2. Flexural Test

To measure the bending stiffness, a four-point bending test was conducted as per ASTM D7249 [22] on corrugated core and sandwich panel specimens, as shown in Figure 3c,d, respectively. The bending specimens were cut in the longitudinal direction of the panel with the width of one UC. As per the standards, five specimens of each panel were tested. The bending stiffness (*EI*) was determined using Equation (3) and load-deflection results obtained from the bending test.

$$EI = \frac{Pa}{48\Delta}(3L^2 - 4a^2) \xrightarrow{a=\frac{L}{3},\ m=\frac{P}{\Delta}} EI = \frac{23mL^3}{1296} \quad (3)$$

where P, Δ, L, and a are bending load, deflection at mid-span, span length, and distance of loading point from the support, respectively. The configuration of the bending test is shown in Figure 4. Table 1 summarizes the dimensions of all flexural test specimens. Note that the specimen length in Table 1 indicates the span length and does not include a 25.5-mm overhang at each end of the flexural specimens (i.e., total length of these specimens was 51 mm longer than span length). Deflection was measured using a ±25-mm linear variable differential transformer (LVDT), located at the mid-span of the test specimens.

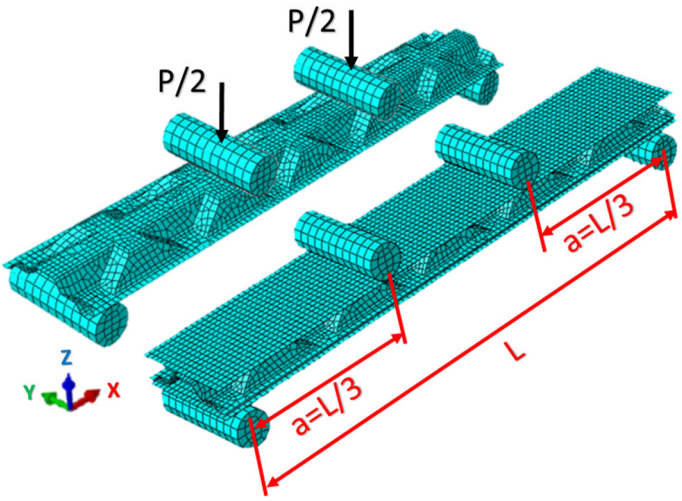

Figure 4. Finite element (FE) model of 3-D core and sandwich panel in the longitudinal direction.

Table 1. Dimensions of flexural specimens used in the bending test.

Specimen	Length L (mm)	Width b (mm)	Thickness t (mm)	Height h (mm)	
Corrugated Core	572	108	6	25	
Sandwich Panel	559	108	---	38	

4. Finite Element Model

To evaluate the bending behavior of both the sandwich panel and the corrugated core within the elastic region, FE models were developed using Abaqus finite element software (Figure 4). For both the flat outer layers and the core, shell elements (S4R) with hourglass control and a reduced integration rule were employed. To easily assign material orientation to the core with complex geometry, a shell element was chosen. Since this type of element considerably decreases the simulation and running time of the FE model, a finer mesh was adopted to increase the accuracy. In addition, all elements were given the capability to undergo finite strains and rotations.

Considering the fabrication process, both the corrugated core and the flat outer plies were assumed to be transversely isotropic. To simulate a perfect bond between the face-sheets and the 3-D core, rigid links were modeled between the nodes of these two components using a tie constraint. As for the boundary conditions, the nodes in the contact area between the specimens and the supports were constrained in the z direction. Since the supports were free to rotate about the y axis to be consistent with ASTM D7249 [22], no other boundary condition was applied. However, to avoid instability in the structure, the centerline of the sandwich panel exactly at the mid-span was fixed to avoid any translation in the x direction. Loading was applied as prescribed downward deflection of the loading heads.

To determine an acceptable element size, a mesh convergence analysis was performed on the flexural 3-D core model. In Figure 5, the results of this convergence study are displayed, comparing the bending load that corresponds to a deflection of 25.4 mm in the center of the specimen to the number of elements. As the number of elements increased from 4263 to 59,814 (corresponding to an element size of 5 mm to 1.3 mm), there was a 1.73% change in the resulting bending load. Because of this negligible change in the bending load and noticeable savings in the computation time, the smallest number of elements considered, 4263 (element size of 5 mm), was chosen to mesh the specimens.

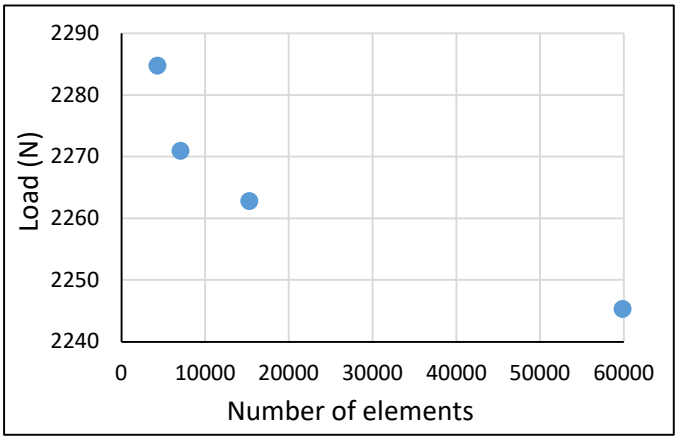

Figure 5. Mesh convergence results of the flexural specimen in the longitudinal direction.

5. Theoretical Model

Due to the complex geometry of a biaxially corrugated core with cavities caused by three-dimensional geometry, it is not easy to develop a theoretical model to capture all deformations under different types of loading. One method to overcome this difficulty is homogenization. In this section, the inhomogeneous sandwich panel with corrugated core geometry is replaced with an equivalent homogenous and continuous layer. The effective properties for this homogenous and continuous layer consist of effective extensional moduli in the x and y directions, effective Poisson's ratio, and effective shear modulus in the x–y plane. Because it is a common practice to compute these effective properties with only consideration of in-plane loading [23–25], they were calculated based on the laminate extensional stiffness matrix, generally referred to as the [A] matrix. Besides the assumption of neglecting resultant moments to calculate effective properties, in developing the theoretical model, all stresses through the thickness were also neglected. Additionally, the [A] matrix components were computed by integrating over the UC volume instead of UC height.

The constitutive equation for a laminate in terms of resultant forces [N], resultant moments [M], mid-plane strains {ε^0}, and mid-plane curvatures {κ} can be written as

$$\begin{Bmatrix} N \\ M \end{Bmatrix} = \begin{bmatrix} A & B \\ B & D \end{bmatrix} \begin{Bmatrix} \varepsilon^0 \\ \kappa \end{Bmatrix} \tag{4}$$

where A, B, and D are the extensional stiffness, the bending–extension coupling, and the bending stiffness matrices, respectively, and their components are defined as

$$A_{ij} = \int_{-h/2}^{h/2} Q_{ij} dz, \quad B_{ij} = \int_{-h/2}^{h/2} Q_{ij} z dz, \quad D_{ij} = \int_{-h/2}^{h/2} Q_{ij} z^2 dz \tag{5}$$

The symmetric and balanced configuration of the sandwich panel about its mid-plane results in a zero bending–extension coupling matrix, [B] (see Appendix). In addition, because the sandwich panel was assumed to be a simplified 2-D structure and evaluated like a plate, all stresses through the thickness were neglected. Therefore, the constitutive equation for the sandwich panel is defined [23] as

$$\begin{Bmatrix} N_x \\ N_y \\ N_{xy} \end{Bmatrix} = \begin{bmatrix} A_{11} & A_{12} & 0 \\ A_{12} & A_{22} & 0 \\ 0 & 0 & A_{66} \end{bmatrix} \begin{Bmatrix} \varepsilon_x^0 \\ \varepsilon_y^0 \\ \gamma_{xy}^0 \end{Bmatrix} \tag{6}$$

and the components of the extensional stiffness matrix ([A]) given in Equation (2) expanded over three layers can be rewritten as

$$A_{ij} = \int_{-h/2}^{h/2} Q_{ij} dz = \left(\int_{-h_f/2}^{h_f/2} Q_{ij} dz \right)_{Top} + \left(\int_{-h_c/2}^{h_c/2} Q_{ij} dz \right)_{Core} + \left(\int_{-h_f/2}^{h_f/2} Q_{ij} dz \right)_{Bottom} \tag{7}$$

where Q_{ij} are components of the stiffness matrix in the global coordinate system (x–y–z) [26]. Additionally, h_f is the thickness of the outer layers and h_c is the height of the corrugated core. For

uniaxial corrugated cores, such as those with sinusoidal or trapezoidal configurations where the corrugated geometries can be easily specified with a known function, computing these integrals over the height to calculate the extensional stiffness matrix ([A]) is straightforward [27–29]. However, since the geometry of the core analyzed in this study is biaxially corrugated and varies along both the x and y axes, the second term in Equation (7) representing the core layer cannot be easily computed. Unlike other methods which use a known function describing the core geometry to compute Equations (5) and (7), a discretization technique was used to simplify the integration in this study. Therefore, one quarter of the UC (Figure 2b) was broken down into seven simplified domains as shown in Figure 2b. Subsequently, integration was carried out over the simplified domains and averaged as

$$\int_{-h_c/2}^{h_c/2} Q_{ij}\,dz = \frac{4}{L_1L_2}\int_0^{\frac{L_1}{2}}\int_0^{\frac{L_2}{2}}\int_{-h_c/2}^{h_c/2} Q_{ij}\,dz\,dy\,dx = \frac{4}{L_1L_2}\sum_{k=1}^{7}\left(\int_{V_k} Q_{ij}\,dV\right) \tag{8}$$

where L_1 and L_2 are dimensions of the unit cell, and V_k is volume of each domain shown in Figure 2b.

It should be noted that the components of the global stiffness matrix (Q_{ij}) of the core layer given in Equations (7 and 8) are obtained by transforming the stiffness matrix in the local coordinate system (1–2–3) using the transformation matrix, [T]. Considering the global coordinate system (x–y–z) and local coordinate system (1–2–3) that varies from domain to domain, the transformation matrix for each domain is expressed as

$$\text{For domain \#1, 3, 5, 7:}\quad T = \begin{bmatrix} 1 & 0 & 0 & 0 & 0 & 0 \\ 0 & m^2 & n^2 & 0 & 2mn & 0 \\ 0 & n^2 & m^2 & 0 & -2mn & 0 \\ 0 & 0 & 0 & m^2-n^2 & 0 & 0 \\ 0 & -mn & mn & 0 & m & -n \\ 0 & 0 & 0 & 0 & n & m \end{bmatrix},\quad \begin{cases} m = \cos(0) \\ n = \sin(0) \end{cases}$$

$$\text{For domain \#4:}\quad T = \begin{bmatrix} m^2 & 0 & n^2 & 0 & 2mn & 0 \\ 0 & 1 & 0 & 0 & 0 & 0 \\ n^2 & 0 & m^2 & 0 & -2mn & 0 \\ 0 & 0 & 0 & m & 0 & -n \\ -mn & 0 & mn & 0 & m^2-n^2 & 0 \\ 0 & 0 & 0 & n & 0 & m \end{bmatrix},\quad \begin{cases} m = \cos(30) \\ n = \sin(30) \end{cases} \tag{9}$$

$$\text{For \#2 and 6:}\quad T = \begin{bmatrix} m^2 & n^2 & 0 & 0 & 0 & 2mn \\ n^2 & m^2 & 0 & 0 & 0 & -2mn \\ 0 & 0 & 1 & 0 & 0 & 0 \\ 0 & 0 & 0 & m & -n & 0 \\ 0 & 0 & 0 & n & m & 0 \\ -mn & mn & 0 & 0 & 0 & m^2-n^2 \end{bmatrix},\quad \begin{cases} m = \cos(56) \\ n = \sin(56) \end{cases}$$

and inverting the extensional stiffness matrix ([A]) in Equation (6) results in

$$\begin{Bmatrix} \varepsilon_x^0 \\ \varepsilon_y^0 \\ \gamma_{xy}^0 \end{Bmatrix} = \begin{bmatrix} A_{11} & A_{12} & 0 \\ A_{12} & A_{22} & 0 \\ 0 & 0 & A_{66} \end{bmatrix}^{-1} \begin{Bmatrix} N_x \\ N_y \\ N_{xy} \end{Bmatrix} = \begin{bmatrix} a_{11} & a_{12} & 0 \\ a_{12} & a_{22} & 0 \\ 0 & 0 & a_{66} \end{bmatrix} \begin{Bmatrix} N_x \\ N_y \\ N_{xy} \end{Bmatrix} \quad . \tag{10}$$

The stress-strain relation for a homogenous and continuous lamina with the thickness of h is expressed as

$$\begin{Bmatrix} \varepsilon_x^0 \\ \varepsilon_y^0 \\ \gamma_{xy}^0 \end{Bmatrix} = \begin{bmatrix} 1/E_{\mathrm{x}} & -\upsilon_{\mathrm{xy}}/E_{\mathrm{x}} & 0 \\ -\upsilon_{\mathrm{yx}}/E_{\mathrm{y}} & 1/E_{\mathrm{y}} & 0 \\ 0 & 0 & 1/G_{\mathrm{xy}} \end{bmatrix} \begin{Bmatrix} \sigma_{\mathrm{x}} \\ \sigma_{\mathrm{y}} \\ \tau_{\mathrm{xy}} \end{Bmatrix} = \frac{1}{h} \begin{bmatrix} 1/E_{\mathrm{x}} & -\upsilon_{\mathrm{xy}}/E_{\mathrm{x}} & 0 \\ -\upsilon_{\mathrm{yx}}/E_{\mathrm{y}} & 1/E_{\mathrm{y}} & 0 \\ 0 & 0 & 1/G_{\mathrm{xy}} \end{bmatrix} \begin{Bmatrix} N_x \\ N_y \\ N_{xy} \end{Bmatrix} \tag{11}$$

and comparing Equation (10) for the biaxial corrugated core sandwich panel with Equation (11) for a lamina gives the effective material properties of a lamina that is equivalent to the biaxial corrugated core sandwich panel. These material properties are summarized [23] as

$$E_x = 1/h\,a_{11},\quad E_y = 1/h\,a_{22},\quad G_{xy} = 1/h\,a_{66},\quad \nu_{xy} = -a_{12}/a_{11},\quad \nu_{yx} = -a_{12}/a_{22} \tag{12}$$

Considering these effective material properties, two different beam models, classical beam theory (Euler–Bernoulli) and first-order shear deformation beam theory (Timoshenko), were employed to investigate the bending behavior of the equivalent structure. Using displacement fields of these beam models, the principle of minimum potential energy, and the variational method, the governing equations for this sandwich beam [30,31] were derived as

$$\text{Euler–Bernoulli:}\quad Q_{11}I\frac{\partial^4 w}{\partial x^4} = q(x)$$

$$\text{Timoshenko:}\quad \begin{cases} Q_{11}I\frac{\partial^2 \phi}{\partial x^2} - k_s Q_{55}A\left(\phi_x + \frac{\partial w}{\partial x}\right) = 0 \\ k_s Q_{55}A\left(\frac{\partial^2 w}{\partial x^2} + \frac{\partial \phi}{\partial x}\right) + q(x) = 0 \end{cases} \tag{13}$$

where beam deflection and rotation of the cross section about the y axis with respect to the thickness direction are shown with w and ϕ respectively. Additionally, Q_{11} and Q_{55}, k_s, A, and I, which are components of the stiffness matrix of the homogenized beam, shear correction factor, cross section area, and moment of inertia, respectively, are given as

$$\begin{gathered} Q_{11} = E_x/(1-\nu_{xy}\nu_{yx}) \qquad \text{and} \qquad Q_{55} = G_{13} \\ I = \frac{1}{12}bh^3, \qquad A = bh, \qquad k_s = (5+5\nu_{xy})/(6+5\nu_{xy}) \end{gathered} \tag{14}$$

As shown in Table 1, b and h are the width and the height of the sandwich panel test specimen and the material properties are given in Equation (12). It should be noted that effective out-of-plane shear modulus (G_{13}) is assumed equal to that of in-plane shear modulus (G_{12}) [23]. Since Fourier series expansions satisfy the boundary conditions [32], they were used to solve the governing equation(s). Based on Euler–Bernoulli and Timoshenko beam theories, the closed form solution for the deflection of this sandwich beam with biaxial corrugated geometry under a four-point bending test, as shown in Figure 4, is obtained as:

$$\text{Euler–Bernoulli:}\quad w(x) = \sum_{n=1}^{\infty} \frac{\mathrm{p}L^3\left(sin\left(\frac{n\pi a}{\mathrm{L}}\right)+sin\left(\frac{n\pi(x-a)}{\mathrm{L}}\right)\right)}{Q_{11}I(n\pi)^4} sin\left(\frac{n\pi x}{L}\right)$$

$$\text{Timoshenko:}\quad w(x) = \sum_{n=1}^{\infty}\left[\frac{(Q_{11}I(n\pi)^2+k_sQ_{55}AL^2)PL\left(sin\left(\frac{n\pi}{3}\right)+sin\left(\frac{2n\pi}{3}\right)\right)}{k_sQ_{55}Q_{11}IA(n\pi)^4}\right] sin\left(\frac{n\pi x}{L}\right) \tag{15}$$

6. Results and Discussion

Results of tensile testing were used to obtain the elastic constants of the wood composite material. Using these properties, FE and theoretical models to investigate the bending behavior were applied and their results were compared with experimental results.

6.1. Elastic Constants

To establish the properties of the wood composite material, 19 coupons were tested at each angle (0°, 15°, and 90°). A typical stress–strain curve, along with the failure mode, of a tensile coupon is presented in Figure 6. Since the stress–strain curve is almost linear, as proven by the regression model (red dotted line) and the coefficient of determination (R^2), material nonlinearity for this wood composite sandwich panel can be ignored. Density plays an important role in affecting stress–strain curve and load-carrying capacity of this composite material. Therefore, test results of those coupons with a density of around 640 (kg/m^3) were chosen to obtain the material properties. This avoided any variation caused by the density. All panels were manufactured to a target density of 640 kg/m^3 in this study, since this density has been used for similar wood-strand products [11–14,18] and also is a typical average density for commercially available OSB [20]. These material properties are summarized in Table 2 and coefficients of variation in percent are presented in parentheses.

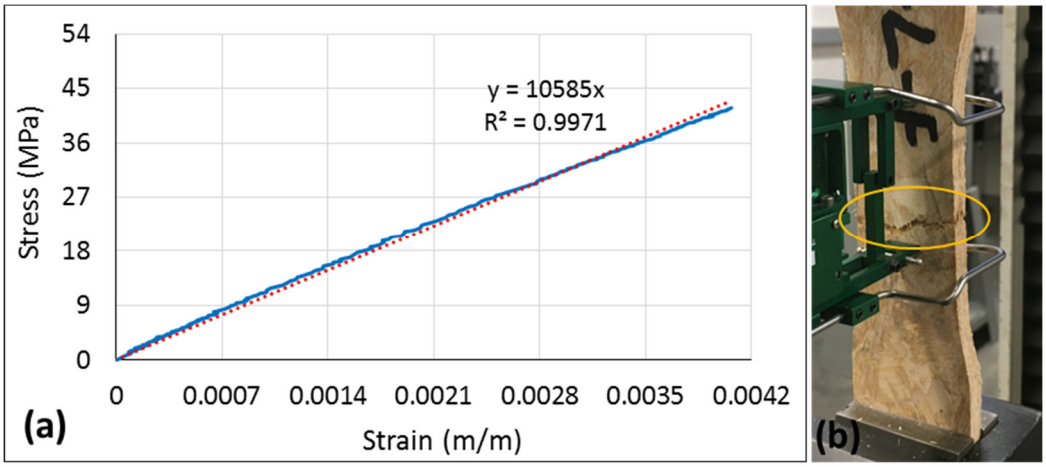

Figure 6. Typical results of tensile testing: (**a**) load–strain graph (blue line) along with regression model (red dotted line), (**b**) failure mode.

Table 2. Elastic constants of wood strand composite material. Values in parenthesis are COVs in percent.

E_1 (GPa)	E_2 (GPa)	G_{12} (GPa)	ρ (kg/m³)
9.80 (9.4%)	1.71 (13.4%)	2.56 (37.8%)	640

Variation in material properties is to be expected in all heterogeneous and anisotropic materials, as can be seen in coefficient of variation values in Table 2. As explained, this is especially true for wood. For wood-based products, variation in density can affect the material properties. The influence of the density on longitudinal Young modulus of the wood strand plies tested in this study is shown in Figure 7. Results indicate that a 46% change in density caused a 107% change in longitudinal Young's modulus.

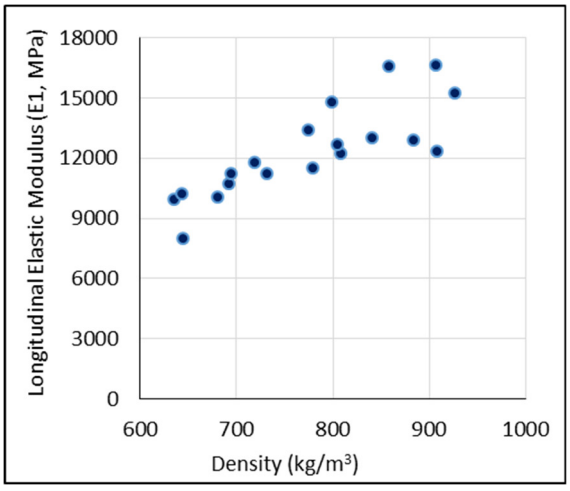

Figure 7. Effect of density on longitudinal Young modulus.

Considering the material properties obtained from tensile testing and the assumption of transverse isotropy, the material properties of the wood strand composite are summarized in Table 3. These elastic constants served as inputs for the FE model as well as for the theoretical model to compute the stiffness matrix in Equation (7).

Table 3. The material properties of specimens.

E_1 (GPa)	E_2 (GPa)	E_3 (GPa)	υ_{12} [18]	υ_{13}	υ_{23} [19]	G_{12} (GPa)	G_{13} (GPa)	G_{23} (GPa)
9.80	1.71	1.71	0.358	0.358	0.2	2.56	2.56	0.71

6.2. Bending Behavior

When subjected to a four-point bending load, the corrugated core specimens in the longitudinal direction failed due to tension, as shown in Figure 8a. Comparison between the average of the experimental results and FE results for deflection in the middle of the specimens subjected to bending is shown in Figure 8b. Since the FE simulation was developed to capture the bending behavior within the linear region, there is a close agreement between these two models in the linear elastic region. The difference between experimental and FE bending stiffness, calculated using Equation (3), within the linear elastic region is 1.4%.

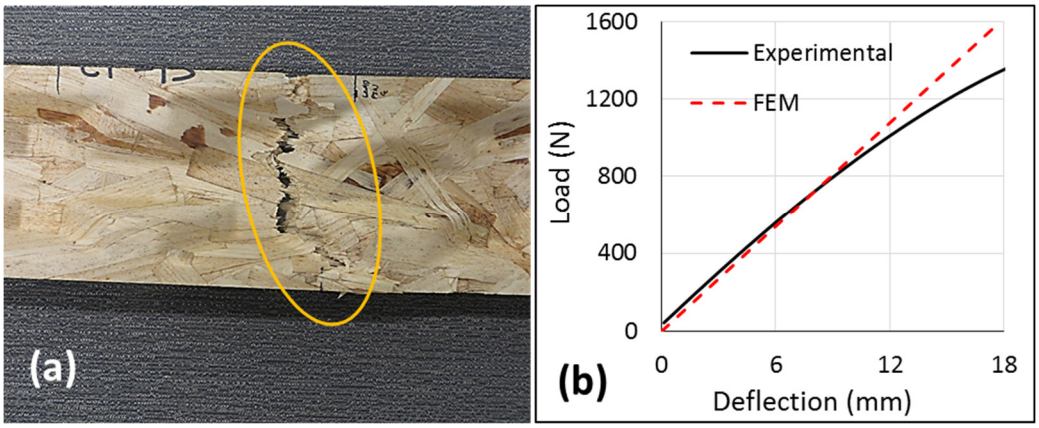

Figure 8. Four-point bending test of the 3-D core layer in the longitudinal (**a**) failure mode (**b**) load–deflection curve.

Sandwich specimens were also subjected to four-point bending, and a typical load–deflection curve and failure mode are presented in Figure 9. Unlike the corrugated core samples, the initial failure mode of longitudinal sandwich panels was debonding between the core and face-sheets (Figure 9b) due to interfacial shear. Bending load versus deflection at the midpoint of these sandwich panels for theoretical and FE models were compared against the average experimental results in Figure 10a. Based on the linear region of these load–deflection curves and Equation (3), the bending stiffness of sandwich beams for different models was calculated and compared in Figure 10b. For experimental results, the bending stiffness was calculated based on the results between 20%–50% of maximum load (i.e., the portion of the curve between about 1000N and 2200N in Figure 10a).

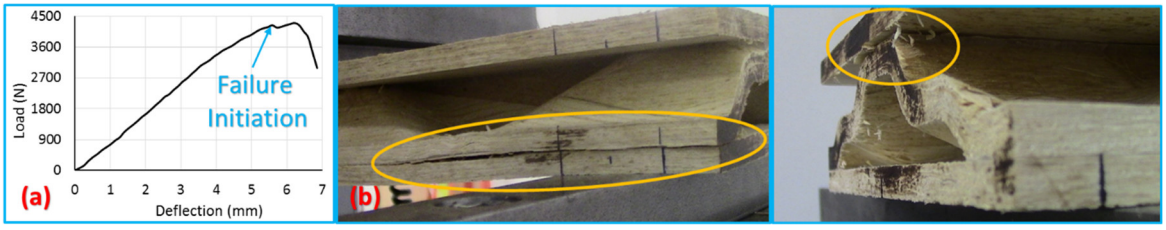

Figure 9. Four-point bending test of the sandwich specimens in the longitudinal direction: (**a**) typical load–deflection curve, (**b**) failure mode, delamination due to interfacial shear between the outer plies and the core.

The difference between experimental and theoretical bending stiffness within the linear elastic region are 3.6% and 5.2% for sandwich beams based on Euler–Bernoulli and Timoshenko models,

respectively. Assumptions in the theoretical models could be the sources of error when compared against the experimental results. These assumptions include considering the composite panel as a beam instead of a plate to develop the theoretical model; this results in neglecting any deformation in the y direction, and ignoring both shear and normal stresses through the thickness by assuming the sandwich panel as a simplified 2-D structure to compute the effective properties. The difference between the Timoshenko beam model, which considers shear deformation, and the Euler–Bernoulli beam model, which does not consider this deformation, is not noticeable within the elastic region. Neglecting shear and normal stresses to compute effective properties as explained can be an explanation for this small difference. However, this difference can be noticeable if these two theories are used to model non-linear behavior. As the theoretical results obtained from both models are generally conservative compared to the experimental ones, the theoretical model can be a good predictive model to use in design of new geometry; however, it is limited to predicting the elastic behavior.

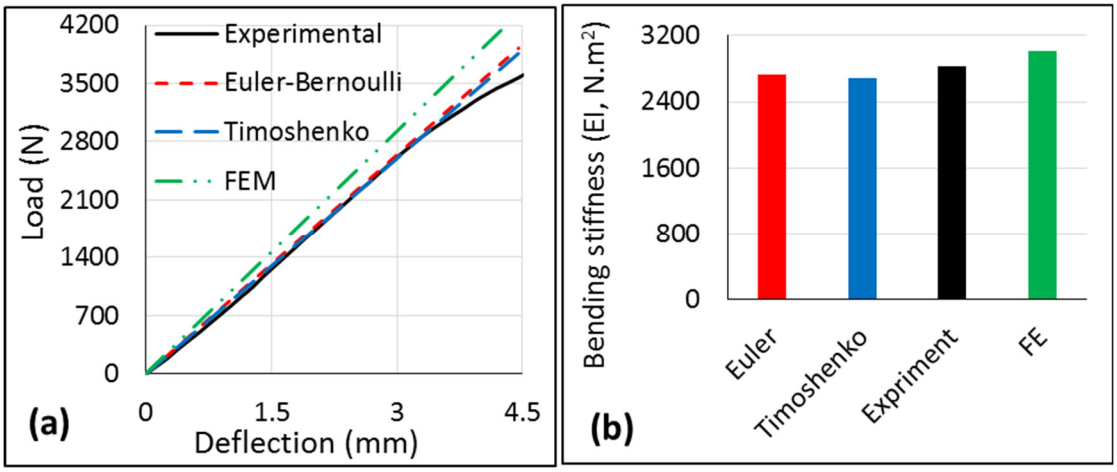

Figure 10. Comparison of (**a**) load–deflection curve and (**b**) bending stiffness of sandwich beams under bending load as shown in Figure 3d based on different models.

Bending stiffness predicted by the FE model differs by 6.5% compared to the experimental results. This slightly larger difference compared to the theoretical bending stiffness could be due to the rigid link used for modeling the bonding area between the core and outer layers. Failure initiation for sandwich specimens started at the bonding area, which results in the failure mode of delamination in that area, as shown in Figure 9b. However, this bonding area was not modeled in the FE simulation and the rigid link, which does not undergo any deformation, was used to bond the core to face-sheets. Therefore, the FE model experiences less deformation compared to the actual one, and results in a higher bending stiffness. The deflected shapes of the FE simulation of the corrugated core and sandwich panel subjected to a four-point bending test, which were used to obtain the results presented in Figures 8b and 10, are shown in Figure 11.

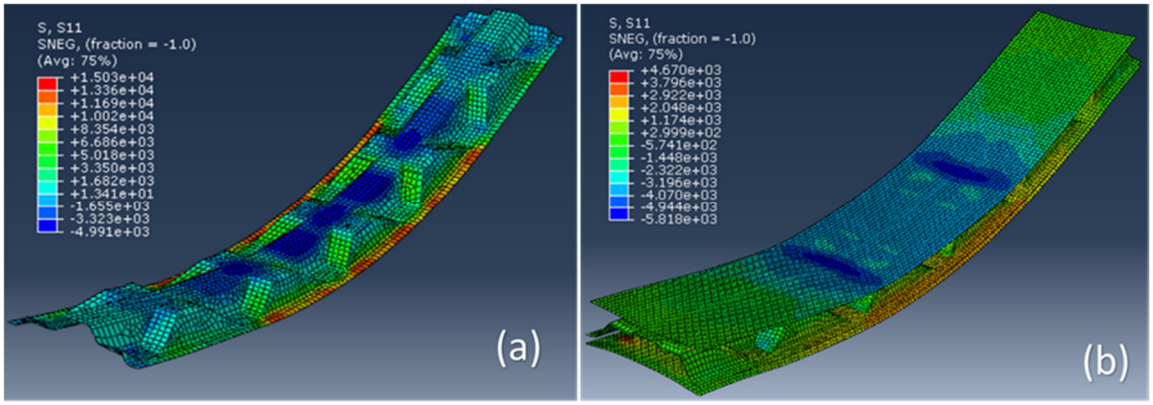

Figure 11. Deformed shape of the FE model of (**a**) 3D core and (**b**) sandwich panel.

Another explanation for the difference between model results and the experimental results could be the variation in material properties. Material properties shown in Tables 2 and 3, which were used to develop both the theoretical and FE models, were established considering the tensile test results of coupons with a density of 640 kg/m^3. However, since there is always a variation between the target density that a panel is pressed to and the actual density, the bending behavior from panel to panel and even from specimen to specimen within a same panel could vary. Therefore, predictions of bending stiffness by these two models could be expected to vary from the experimental results, especially in the case of wood-based materials.

7. Sensitivity Analysis

Intrinsic variation in material properties of wood strands, inconsistencies in the fabrication process, and variations in density may influence the material properties of the wood strand composite panels, as shown in the results so far. Even with extreme care during the fabrication process and the testing, there still will be noticeable variation in the material properties determined (reflected by the coefficient of variations in Table 2). Such a variation leads to variation in the bending stiffness of the sandwich panel and its components. In this section, a sensitivity analysis is presented to clarify the extent of variation in bending stiffness that could be expected due to specified variation in material properties. To this end, using the FE simulation and theoretical model, one material property was changed while others were held constant, and then change in the bending stiffness of the sandwich specimen due to change in the material property was obtained. The coefficient of variation (COV) for each property listed in Table 2 was used as a guide to vary a material property to perform the sensitivity analysis. Results of the sensitivity analysis are given in Table 4. Based on COVs listed in Table 2, e.g., the longitudinal Young's modulus (E_1) was varied by ±9.4%, and the bending stiffness was computed using FE and theoretical models. A 9.4% increase in E_1 indicates an increase of 8.5%, 9.3%, and 9.2% in FE, Euler–Bernoulli, and Timoshenko bending stiffness, respectively. Meanwhile, a 9.4% reduction in E_1 shows a decrease of 8.7%, 9.2%, and 9.1% in FE, Euler–Bernoulli, and Timoshenko bending stiffness. However, a higher change in E_2, ±13.4%, creates less than ±1% change in both FE and the theoretical bending stiffness. Theoretical bending stiffness is not as sensitive as that of FE to change in shear modules because the effects of shear stresses and deformation through the thickness of the panel to calculate effective properties, which were used to develop the theoretical model, were neglected.

Table 4. Percent variation in the longitudinal bending stiffness of the sandwich panel caused by change in material properties.

Property	% Change in Material Properties		% Change in Bending Stiffness		
			FE	Euler	Timoshenko
E1	9.4%	increase: E_1=10.72 GPa	8.8	9.3	9.2
	9.4%	decrease: E_1=8.88 GPa	−8.7	−9.2	−9.1
E2 = E3	13.4%	increase: E_2=1.94 GPa	0.41	0.89	0.34
	13.4%	decrease: E_2=1.48 GPa	−0.5	−0.85	−0.25
G12 = G13	37.8%	increase: G_{12}=3.53 GPa	3.3	0.57	0.97
	37.8%	decrease: G_{12}=1.59 GPa	−5.9	−0.47	−1.5

8. Conclusions

Theoretical and finite element models were developed and applied to predict the linear flexural behavior of the sandwich panel with a complex three-dimensional core geometry manufactured from small-diameter timber under a four-point bending load. The material properties were measured to input into the models.

The bending stiffness of just the corrugated core specimens obtained by the FE model showed a 1.4% difference from the average of the experimental results. In case of the sandwich panel, the average experimental bending stiffness differed from Euler-Bernoulli, Timoshenko, and FE predictions by 3.6%, 5.2%, and 6.5%, respectively. The results indicated that a 46% increase in material density increases the longitudinal Young's modulus by as much as 107%. A sensitivity analysis to understand the effect of variations in material properties on composite sandwich bending stiffness revealed that the longitudinal Young's modulus is the most important property that influences the bending stiffness.

Theoretical and FE models developed for the wood strand sandwich panel were utilized to conduct a parametric study [33] to understand the influence of the core geometry on the bending stiffness of the sandwich panel. Based on the results, new core geometry with higher performance was designed to meet the structural performance requirements of building envelope components, such as wall, floor, and roof. Theoretical models for the sandwich structure with new core geometry were developed for beam [34] and plate [35] configurations.

Author Contributions: Conceptualization, V.Y.; methodology, M.M., J.J. and V.Y.; software, M.M. and J.J.; validation, M.M. and J.J.; formal analysis, M.M., J.J. and V.Y.; investigation, M.M., J.J. and V.Y.; resources, V.Y.; data curation, V.Y.; writing—original draft preparation, M.M. and J.J.; writing—review and editing, V.Y. and W.C.; visualization, M.M. and J.J.; supervision, V.Y.; project administration, V.Y.; funding acquisition, V.Y. All authors have read and agreed to the published version of the manuscript.

Funding: This research was funded by the National Science Foundation, grant number CMMI-1150316.

Conflicts of Interest: The authors declare no conflict of interest.

Appendix

Components of bending–extension coupling matrix ([B]) given in Equation (5) can be written as

$$B_{ij} = \int_{-h/2}^{h/2} Q_{ij} z dz = \left(\int_{-h_f/2}^{h_f/2} (Q_{ij} z) dz\right)_{Top} + \left(\int_{-h_c/2}^{h_c/2} (Q_{ij} z) dz\right)_{Core} + \left(\int_{-h_f/2}^{h_f/2} (Q_{ij} z) dz\right)_{Bottom} \quad \text{(A1)}$$

where h, h_f, and h_c are thickness of the sandwich panel, face-sheets, and core, respectively. Top and bottom subscripts refer to the top and bottom face-sheets. The first and third terms in Equation (A1) (top and bottom) are zero because of the symmetric and balanced configuration of the face-sheets and can be written as

$$\int_{-h_f/2}^{h_f/2} (Q_{ij} z) dz = Q_{ij} \left(\frac{z^2}{2}\right)\Big|_{z=-h_f/2}^{z=h_f/2} = 0 \quad \text{(A2)}$$

Based on Figure 2, the second term, representing the corrugated core, can be written as

$$\int_{-h_c/2}^{h_c/2} Q_{ij} z dz = \frac{4}{L_1 L_2} \int_0^{\frac{L_1}{2}} \int_0^{\frac{L_2}{2}} \int_{-h_c/2}^{h_c/2} (Q_{ij} z) dz dy dx = \frac{4}{L_1 L_2} \left[\left(\iiint (Q_{ij} z) dz dy dx\right)_1 + \left(\iiint (Q_{ij} z) dz dy dx\right)_2 + \left(\iiint (Q_{ij} z) dz dy dx\right)_3 + \left(\iiint (Q_{ij} z) dz dy dx\right)_4 + \left(\iiint (Q_{ij} z) dz dy dx\right)_5 + \left(\iiint (Q_{ij} z) dz dy dx\right)_6 + \left(\iiint (Q_{ij} z) dz dy dx\right)_7 \right] \quad \text{(A3)}$$

Subscripts 1 to 7 represent the segmented parts of the corrugated core as shown in Figure 2b, which are used as the domain for integration. Because of the symmetric and balanced configuration of UC, parts 1 and 7, parts 2 and 6, and parts 3 and 5 cancel out each other. Part 4 is zero on its own because of its symmetric geometry about the mid plane. Therefore, the bending–extension coupling matrix (matrix [B]) for this sandwich panel is zero.

References

1. Pandey, K.K.; Ramakantha, V.; Chauhan, S.S.; Kumar, A.A. *Wood is Good*; Springer: Singapore, 2017.

2. Guy-Quint, C.; Beyer, G.; Defays, M.; Fischer, M.; De Munck, E.; De Jaeger, F.; Van Riet, C.; Vandeweghe, K.; Wijnendaele, K. *Tackle Climate Change: Use Wood*; CEI-Bois, the European Confederation of Woodworking Industries: Brussels, Belgium, 2006.
3. LeVan-Green, S.L.; Livingston, J. Exploring the uses for small-diameter trees. *For. Prod. J.* **2001**, *51*, 10–21.
4. Davies, J.M. *Lightweight Sandwich Construction*; John Wiley & Sons: Hoboken, NJ, USA, 2008.
5. Smardzewski, J. Experimental and numerical analysis of wooden sandwich panels with an auxetic core and oval cells. *Mater. Des.* **2019**, *183*, 108–159.
6. Klímek, P.; Wimmer, R.; Brabec, M.; Sebera, V. Novel sandwich panel with interlocking plywood kagome lattice core and grooved particleboard facings. *BioResources* **2016**, *11*, 195–208.
7. Labans, E.; Kaspars K. Experimental validation of the stiffness optimisation for plywood sandwich panels with rib-stiffened core. *Wood Res.* **2014**, *59*, 793–802.
8. Banerjee, S.; Bhattacharyya, D. Optimal design of sandwich panels made of wood veneer hollow cores. *Compos. Sci. Technol.* **2011**, *71*, 425–432.
9. Kavermann, S.W.; Bhattacharyya, D. Experimental investigation of the static behaviour of a corrugated plywood sandwich core. *Compos. Struct.* **2019**, *207*, 836–844.
10. Hunt, J.F.; Winandy, J.E. 3D engineered fiberboard: A new structural building product. In Proceedings of the Sixth Panel Products Symposium, Llandudno, Wales, UK, 1–11 October 2002; The BioComposites Centre: Bangor, UK, 2002; pp. 106–117.
11. Voth, C.; White, N.; Yadama, V.; Cofer, W. Design and evaluation of thin-walled hollow-core wood-strand sandwich panels. *J. Renew. Mater.* **2015**, *3*, 234–243.
12. White, N.B. Strategies for Improving Thermal and Mechanical Properties of Wood-Composites. Master's Thesis, Washington State University, Pullman, WA, USA, 2011.
13. Mohammadabadi, M.; Yadama V.; Geng J. Creep behavior of 3D core wood-strand sandwich panels. *Holzforschung* **2018**, *72*, 513–519.
14. Mohammadabadi, M.; Yadama, V.; Yao, L.; Bhattacharyya, D. Low-velocity impact response of wood-strand sandwich panels and their components. *Holzforschung* **2018**, *72*, 681–689.
15. Jones, R.M. *Mechanics of Composite Materials*; CRC Press: Boca Raton, FL, USA, 1998.
16. Yadama, V.; Wolcott, M.P.; Smith, L.V. Elastic properties of wood-strand composites with undulating strands. *Compos. Part A: Appl. Sci.***2006**, *37*, 385–392.
17. American Society for Testing and Materials (ASTM). *Standard Test Method for Properties of Wood-Based Fiber and Particle Panel Materials*; ASTM-D1037; ASTM: West Conshohocken, PA, USA, 2006.
18. Weight, S.W. A Novel Wood-Strand Composite Laminate Using Small-Diameter Timber. Master's Thesis, Washington State University, Pullman, WA, USA, 2007.
19. Clouston, P.L. Computational Modeling of Strand-Based Wood Composites in Bending. Ph.D. Thesis, University of British Columbia, Vancouver, BC, Canada, 2001.
20. Ross, R.J. *Wood Handbook: Wood as an Engineering Material*; General Technical Report FPL-GTR-190; USDA Forest Service, Forest Products Laboratory: Madison, WI, USA, 2010.
21. Kamke, F.A. *Physics of hot pressing. Proceedings of Fundamentals of Composite Processing*; General Technical Report FPL-149; USDA Forest Service, Forest Products Laboratory: Madison, WI, USA, 2004; pp. 3–18.
22. American Society for Testing and Materials (ASTM). *Standard Test Method for Facing Properties of Sandwich Constructions by Long Beam Flexure*; ASTM D 7249/D7249 M-06; ASTM: West Conshohocken, PA, USA, 2006.
23. Carlsson, L.A.; Kardomateas, G.A. *Structural and Failure Mechanics of Sandwich Composites*; Springer Science & Business Media: Netherlands, 2011.
24. Hyer, M.W.; White, S.R. *Stress Analysis of Fiber-Reinforced Composite Materials*; DEStech Publications, Inc.: Lancaster, PA, USA, 2009.
25. Aboura, Z.; Talbi, N.; Allaoui, S; Benzeggagh, M.L. Elastic behavior of corrugated cardboard: experiments and modeling. *Compos. Struct.* **2004**, *63*, 53–62.
26. Gibson, R.F. *Principles of Composite Material Mechanics*; CRC Press: Hoboken, NJ, USA, 2016.
27. Magnucka-Blandzi, E.; Magnucki, K.; Wittenbeck, L. Mathematical modeling of shearing effect for sandwich beams with sinusoidal corrugated cores. *Appl. Math. Model.* **2015**, *39*, 2796–2808.
28. Cheon, Y.J.; Kim, H.G. An equivalent plate model for corrugated-core sandwich panels. *J. Mech. Sci. Technol.* **2015**, *29*, 1217–1223.
29. Magnucki, K.; Jasion, P.; Krus, M.; Kuligowski, P.; Wittenbeck, L. Strength and buckling of sandwich beams with corrugated core. *J. Theor. Appl. Mech.* **2013**, *51*, 15–24.

30. Abadi, M.M.; Daneshmehr, A.R. An investigation of modified couple stress theory in buckling analysis of micro composite laminated Euler–Bernoulli and Timoshenko beams. *Int. J. Eng. Sci.* **2014**, *75*, 40–53.
31. Wang, C.M.; Reddy, J.N; Lee, K.H. *Shear Deformable Beams and Plates: Relationships with Classical Solutions*; Elsevier: Oxford, UK, 2000.
32. Daneshmehr, A.R.; Abadi, M.M; Rajabpoor, A. Thermal effect on static bending, vibration and buckling of Reddy beam based on modified couFple stress theory. *Appl. Mech. Mater.* **2013**, *332*, 331–338.
33. Mohammadabadi, M.; Yadama, V. Influence of a Biaxially Corrugated Core Geometry on Flexural Stiffness of Wood-Strand Composite Sandwich Panels. *Mater. Today Commun.* **2020**, 100931. DOI: 10.1016/j.mtcomm.2020.100931
34. Mohammadabadi, M.; Yadama, V.; Smith, L. An analytical model for wood composite sandwich beams with a biaxial corrugated core under bending. *Compos. Struct*. **2019**, 228, 111316. DOI: 10.1016/j.compstruct.2019.111316
35. Mohammadabadi, M.; Yadama, V.; Smith, L. The effect of plate theories and boundary conditions on the bending behavior of a biaxial corrugated core sandwich panel. *Compos. Struct*. **2020**, 228, 112133. DOI: 10.1016/j.compstruct.2020.112133